Journal of Applied Analysis and Computation
Volume 17, Number 1, February 2027, 500–523
Website:http://www.jaac-online.com
DOI:10.11948/20250287

NOVEL EXACT ANALYTICAL SOLUTIONS OF THE (3+1)-DIMENSIONAL POTENTIAL YU-TODA-SASA-FUKUYAMA EQUATION VIA LIE SYMMETRY ANALYSIS AND NEURAL NETWORK MODELS*

Yunjie Yang[1], Jianping Shi[1,†] and Hui Fang[1]

Abstract A novel method combining Lie symmetry analysis and neural network model is proposed for solving the (3+1)-dimensional potential-Yu-Toda-Sasa-Fukuyama (pYTSF) equation in this paper. This method has three processes: Firstly, the dimension of the given equation are reduced and two reduction equations are derived via Lie symmetry analysis; secondly, different test functions are constructed based on neural network models and various activation functions to yield solutions of the reduction equations; finally, a series of exact solutions of the original equation is achieved depending on the expression of group-invariant solutions and the transformation of variables. 12 novel exact analytical solutions of the (3+1)-dimensional pYTSF equation are obtained by the novel method. Furthermore, the dynamical characteristics of all solutions are illustrated by choosing appropriate parameters. The results validate the feasibility of this new method and show that the novel method may be applied in more nonlinear partial differential equations.

Keywords Lie symmetry analysis, neural network model, exact solution, test function, (3+1)-dimensional potential-Yu-Toda-Sasa-Fukuyama equation.

MSC(2010) 70G65, 35A25, 35C10.

1. Introduction

Nonlinear partial differential equations (NLPDEs) have received significant attention from scholars in various fields such as mathematics and physics, because they can describe and explain the ubiquitous nonlinear phenomena in the objective world. Many partial differential equations (PDEs) have been proposed and extensively studied. For example, D. J. Korteweg and G. De Vries proposed the famous shallow water wave equation known as the KdV equation and proved the existence of solitary waves mathematically in 1895 [21]. Researchers have introduced and developed a series of effective methods to study NLPDEs over the past one hundred years. They are mainly classified into analytical and numerical methods. Compared with numerical solutions obtained by numerical methods, analytical solutions obtained by analytical method are represented as exact formulas and are used to characterize dynamics more accurately. The

†The corresponding author.
[1]Department of Mathematics, Kunming University of Science and Technology, Kunming, Yunnan 650500, China
*The authors were supported by the National Natural Science Foundation of China (No. 11561034).
Email: yangyunjie0801@stu.kust.edu.cn(Y. Yang), sjp0207@163.com(J. Shi), mathfanghui@sina.com(H. Fang)

classical analytical methods include the inverse scattering transform method [1], Lie group analysis method [18], Darboux transformation method [29], etc. [7,19,23,25,27,28,36,39,42]. Each method possesses distinct merits, but most are only suitable for specific types of equations. There is no universal method applicable to solving NLPDEs so far. On the other hand, using multiple methods to solve specific equations to obtain solutions with different characteristics is also a common solving strategy. For example, a (2+1)-dimensional KP-BBM equation was investigated by employing the Hirota's bilinear and a novel limit method in [42]. In [28], the $tan(\phi/2)$-expansion method, Jacobi elliptic function expansion scheme, rational multi-wave functions, and decomposition variational iteration method were considered to investigate the exact traveling wave solutions to the fourth-order Cahn–Hilliard equation.

In the second half of the 19th century, the Norwegian mathematician Sophus Lie proposed Lie transformation group and symmetry. The central principle is that if an ordinary differential equation (ODE) is invariant under a one-parameter classical Lie group, its order can be reduced by one. For PDE, the number of independent variables can be reduced by one [35]. Lie group analysis has been applied to various differential equations, yielding a wealth of exact solutions. Furthermore, some theorems and methods have been gradually extended, such as Noether's Theorem [30], Lie-Bäcklund symmetry [38] and conditional Lie-Backlund symmetry [54]. In 2013, Bluman et al. introduced a new and complementary method for constructing nonlocal symmetries [4]. In recent years, some scholars have applied machine learning to discover symmetry transformations and acquire new research achievements [11,12].

Artificial neural network (ANN) has been a powerful tool in image processing [3], computer vision [51], oil and gas engineering [6], and other fields in recent years. Some researches tried to utilize ANN for solving differential equations. In 1990, Hornik et al. proved that multilayer feedforward network was capable of approximating arbitrary function and its derivatives [15], which laid the theoretical foundation for neural networks to solve differential equations. However, many methods based on ANN are numerical [14,31,33,37]. In 2019, Runfa Zhang et al. first proposed the bilinear neural network method (BNNM) using the powerful representational capacity of neural networks to derive exact solutions of PDEs [47]. Novel trial functions were constructed in [49]. Furthermore, Runfa Zhang et al. proposed the bilinear residual network method (BRNM), which connected the shallow input jumps to the deeper layer without adding extra parameters and model complexity, increasing the internal interactions of models [48]. Xiaoran Xie et al. proposed an innovative approach combined neural network models and symbolic computing [41].

In 1998, Yu et al. proposed (3+1)-dimensional potential-Yu-Toda-Sasa-Fukuyama (pYTSF) equation guided by the strong symmetry and given the travelling solitary wave solution,

$$u_{xxxz} + 4u_x u_{xz} + 2u_{xx} u_z - 4u_{xt} + 3u_{yy} = 0, \tag{1.1}$$

where $u = u(x, y, z, t)$, subscripts denote the partial derivatives with respect to the spatial variables x, y, z and temporal variable t [44]. Eq. (1.1) describes elastic quasiplane waves in a lattice and interfacial waves in a two-layer fluid system [34]. Researchers have employed various methods to study the Eq. (1.1) and obtained abundant exact solutions: Solutions with arbitrary functions [43], non-travelling wave solutions [50], periodic kink-wave, periodic soliton, and doubly periodic wave solutions [46], among others [9, 13, 16, 17, 22, 26, 40, 52, 53]. Additionally, the generalized (3+1)-dimensional nonlinear pYTSF equation and the (2+1)-dimensional pYTSF equation have been investigated [2,5,8,10,24,45].

For many High-dimensional NLPDEs, deriving exact solutions of reduced equations via Lie symmetry reduction remains challenging due to multi-dimensionality and nonlinearity. Building on the aforementioned research trends, especially inspired by BNNM proposed by Runfa Zhang et al., this paper aims to combine Lie symmetry analysis and neural network models to solve the novel exact solutions of the (3+1)-dimensional pYTSF equation. This new approach named as Lie-symmetry neural network method (LSNNM) brings the following advantages: Firstly, the dimension of the pYTSF equation is reduced through Lie symmetry analysis, which decreases the number of neurons in the input layer of the neural network model and simplifies the difficulty of solving the equation to a certain extent. Secondly, different linear combinations of generators can yield multiple reduction equations and offer greater flexibility in solving the original equations. More importantly, we can obtain abundant new exact solutions through constructing test functions based on different neural network models and activation functions.

This article is organized as follows: In Section 2, the framework of LSNNM and six neural network models are introduced. Meanwhile, the dimension of Eq. (1.1) is reduced by one and two reduction equations are yielded via Lie symmetry analysis. In Section 3, based on six neural network models, we construct distinguishing test functions to solve two reduction equations and thereby derive 12 novel exact solutions of the Eq. (1.1). Furthermore, the dynamics of solutions are visually exhibited by choosing appropriate parameters and the main results are given. In Section 4, we summarize the physical significance of the solutions for pYTSF equation. Moreover, the advantages and the prospects for the future of the new proposed method are analyzed.

2. Preliminaries

2.1. The framework of Lie-symmetry neural network method

The framework of the LSNNM is illustrated in Figure 1:

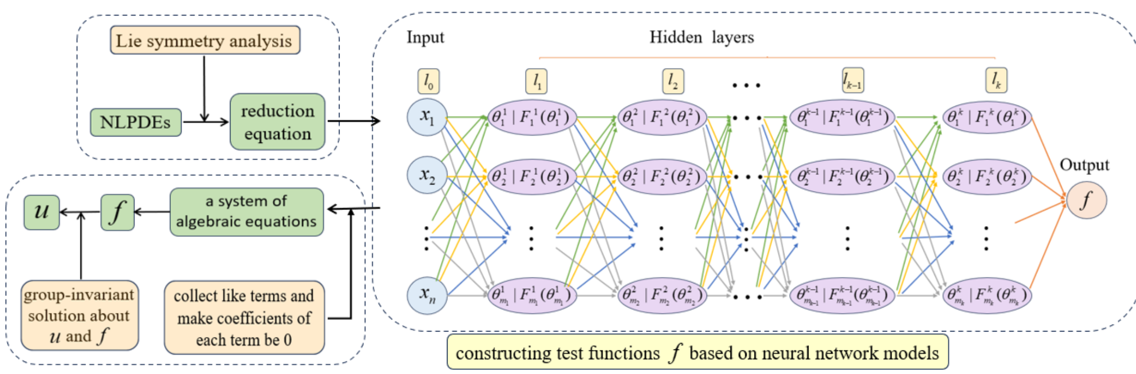

Figure 1. The framework of Lie-symmetry neural network method.

The tensor formula of a $k+2$ level neural network model is given as below:

$$
\begin{aligned}
&\theta_j^1 = \sum w_{i,j}^1 x_i, (i = 1, 2, ..., n, j = 1, ..., m_1),\\
&\theta_j^{s+1} = \sum w_{i,j}^{s+1} F_i^s(\theta_i^s) + b_j^{s+1}, (s = 1, ...k-1, i = 1, ...m_s, j = 1, ..., m_{s+1}),\\
&f = \sum w_i^k F_i^k(\theta_i^k) + b_f, (i = 1, ...m_k),
\end{aligned}
\tag{2.1}
$$

where $w_{i,j}^s$ is the weight coefficient, b_j^s is a bias term. The input layer includes n variables noted as $l_0 = (x_1, x_2, ..., x_n)$, the s-th hidden layer is noted as $l_s = (\theta_1^s, \theta_2^s, ..., \theta_{m_s}^s)(s = 1, 2, ..., k)$, and θ_j^s is the j-th neure and m_i is the number of neuron of the s-th lever. $F_j^s(\cdot)(s = 1, ..., k, j = 1, 2, ..., m_s)$

is the activation function of the j-th neuron of s-th level and the output layer yields test function f finally [48].

In accordance with the framework depicted in Figure 1, the main steps of the approach combining Lie symmetry analysis and neural network models are described in detail below:

Step 1. Lie symmetry analysis of NLPDEs (pYTSF equation in this study). We set a one-parameter Lie group of infinitesimal transformations of the original equations and work out the Lie point symmetry and generators, then verify the closeness of the Lie bracket operation.

Step 2. Yield reduction equations by symmetry reduction. Firstly, select the suitable generators to form linear combinations and get the corresponding characteristic equations. Secondly, determine similarity variables and group-invariant solution expressions. Finally, substitute them into the original equation to generate reduction equations.

Step 3. Construct test function relied on different neural network models and substitute it into the reduction equation to yield a complex equation.

Step 4. Collect like terms and make the coefficients of each term be 0, thus producing a system of algebraic equations with respect to weight and bias.

Step 5. Solve the system of algebraic equations for coefficient solution and bring it back to the test function, thereby deriving solution of the reduction equation.

Step 6. Obtain exact solution of the NLPDE according to the expression of group-invariant solutions and the transformation of variables.

2.2. Lie symmetry reduction

According to the theory and method of Lie symmetry analysis in literature [18], thirteen infinitesimal generators of Eq. (1.1) are achieved as follows:

$$
\begin{aligned}
&X_1 = -x\frac{\partial}{\partial x} + 3z\frac{\partial}{\partial z} + t\frac{\partial}{\partial t} + u\frac{\partial}{\partial u}, \quad X_2 = \frac{\partial}{\partial t}, \quad X_3 = 2x\frac{\partial}{\partial x} + y\frac{\partial}{\partial y} - 4z\frac{\partial}{\partial z} - 2u\frac{\partial}{\partial u},\\
&X_4 = \frac{2y}{3}\frac{\partial}{\partial x} + t\frac{\partial}{\partial y}, \quad X_5 = \frac{\partial}{\partial y}, \quad X_6 = t\frac{\partial}{\partial z} - x\frac{\partial}{\partial u}, \quad X_7 = \frac{\partial}{\partial z}, \quad X_8 = t\frac{\partial}{\partial x} - 2z\frac{\partial}{\partial u},\\
&X_9 = \frac{\partial}{\partial x}, \quad X_{10} = ty\frac{\partial}{\partial u}, \quad X_{11} = y\frac{\partial}{\partial u}, \quad X_{12} = t\frac{\partial}{\partial u}, \quad X_{13} = \frac{\partial}{\partial u}.
\end{aligned} \tag{2.2}
$$

The Lie algebra commutator is defined by $[X_i, X_j] = X_iX_j - X_jX_i$ [18]. It is easy to verified that generators Eq. (2.2) on Lie algebra operations are closed.

Different reduction equations can be derived by generating various linear combinations of some generators, and we focus on two of them in this paper:

Case I. Considering the generator $X_2 + X_5 + X_7 + X_9 + X_{13} = \frac{\partial}{\partial x} + \frac{\partial}{\partial y} + \frac{\partial}{\partial z} + \frac{\partial}{\partial t} + \frac{\partial}{\partial u}$, the corresponding characteristic system is:

$$
\frac{\mathrm{d}x}{1} = \frac{\mathrm{d}y}{1} = \frac{\mathrm{d}z}{1} = \frac{\mathrm{d}t}{1} = \frac{\mathrm{d}u}{1}, \tag{2.3}
$$

then the similarity variables and group-invariant solution are

$$
\chi = -z + x, \quad \eta = -z + y, \quad \tau = -z + t, \quad f = -z + u, \tag{2.4}
$$

and

$$
u = f(\chi, \eta, \tau) + z = f(-z + x, -z + y, -z + t) + z. \tag{2.5}
$$

Substituting (2.5) into Eq. (1.1), one can obtain the reduction equation:

$$(-6f_\chi - 2f_\eta - 2f_\tau + 2)f_{\chi\chi} + (-4f_{\chi\tau} - 4f_{\chi\eta})f_\chi - 4f_{\chi\tau} + 3f_{\eta\eta} - f_{\chi\chi\chi\chi} - f_{\chi\chi\chi\eta} - f_{\chi\chi\chi\tau} = 0. \quad (2.6)$$

Case II. Considering the generator $X_2 + X_5 + X_7 + X_8 = t\frac{\partial}{\partial x} + \frac{\partial}{\partial y} + \frac{\partial}{\partial z} + \frac{\partial}{\partial t} - 2z\frac{\partial}{\partial u}$, the corresponding characteristic system is:

$$\frac{\mathrm{d}x}{t} = \frac{\mathrm{d}y}{1} = \frac{\mathrm{d}z}{1} = \frac{\mathrm{d}t}{1} = \frac{\mathrm{d}u}{-2z}, \tag{2.7}$$

then the similarity variables and group-invariant solution are

$$\chi = -\frac{t^2}{2} + x, \quad \eta = -t + y, \quad \tau = -t + z, \quad f = -t^2 + 2tz + u, \tag{2.8}$$

and

$$u = f(\chi, \eta, \tau) + t^2 - 2tz = f\Big(-\frac{t^2}{2} + x, -t + y, -t + z\Big) + t^2 - 2tz. \tag{2.9}$$

Substituting (2.9) into Eq. (1.1), one can obtain the reduction equation:

$$\big(4f_\chi + 4\big)f_{\chi\tau} + 2f_\tau f_{\chi\chi} + 3f_{\eta\eta} + f_{\chi\chi\chi\tau} + 4f_{\chi\eta} = 0. \tag{2.10}$$

2.3. Neural network models

According to Subsection 2.2, one can obtain the solutions of Eq. (1.1) by solving Eq. (2.6) and Eq. (2.10). As shown in Figure 2, we consider six neural network models and set specific test functions to obtain abundant novel exact solutions for Eq. (1.1) in this paper. The formulas for each model are as follows:

Model [3,2,1]:

$$\begin{aligned} &f = w_{1,f}F_1(\theta_1) + w_{2,f}F_2(\theta_2) + b_3, \\ &\theta_1 = \chi w_{\chi,1} + \eta w_{\eta,1} + \tau w_{\tau,1}, \ \ \theta_2 = \chi w_{\chi,2} + \eta w_{\eta,2} + \tau w_{\tau,2}. \end{aligned} \tag{2.11}$$

Model [3,3,1]:

$$\begin{aligned} &f = w_{1,f}F_1(\theta_1) + w_{2,f}F_2(\theta_2) + w_{3,f}F_3(\theta_3) + b_4, \\ &\theta_1 = \chi w_{\chi,1} + \eta w_{\eta,1} + \tau w_{\tau,1}, \ \ \theta_2 = \chi w_{\chi,2} + \eta w_{\eta,2} + \tau w_{\tau,2}, \\ &\theta_3 = \chi w_{\chi,3} + \eta w_{\eta,3} + \tau w_{\tau,3}. \end{aligned} \tag{2.12}$$

Model [3,1,1,1]:

$$\begin{aligned} &f = w_{2,f}F_2(\theta_2) + b_3, \\ &\theta_2 = w_{1,2}F_1(\theta_1) + b_2, \ \ \theta_1 = \chi w_{\chi,1} + \eta w_{\eta,1} + \tau w_{\tau,1}. \end{aligned} \tag{2.13}$$

Model [3,2,1,1]:

$$\begin{aligned} &f = w_{3,f}F_3(\theta_3) + b_4, \\ &\theta_3 = w_{1,3}F_1(\theta_1) + w_{2,3}F_2(\theta_2) + b_3, \\ &\theta_1 = \chi w_{\chi,1} + \eta w_{\eta,1} + \tau w_{\tau,1}, \ \ \theta_2 = \chi w_{\chi,2} + \eta w_{\eta,2} + \tau w_{\tau,2}. \end{aligned} \tag{2.14}$$

Model [3,2,2,1]:

$$
\begin{aligned}
&f = w_{3,f}F_3(\theta_3) + w_{4,f}F_4(\theta_4) + b_5,\\
&\theta_3 = w_{1,3}F_1(\theta_1) + w_{2,3}F_2(\theta_2) + b_3,\;\; \theta_4 = w_{1,4}F_1(\theta_1) + w_{2,4}F_2(\theta_2) + b_4,\\
&\theta_1 = \chi w_{\chi,1} + \eta w_{\eta,1} + \tau w_{\tau,1},\;\; \theta_2 = \chi w_{\chi,2} + \eta w_{\eta,2} + \tau w_{\tau,2}.
\end{aligned}
\tag{2.15}
$$

Model [3,3,3,1]:

$$
\begin{aligned}
&f = w_{4,f}F_4(\theta_4) + w_{5,f}F_5(\theta_5) + w_{6,f}F_6(\theta_6) + b_7,\\
&\theta_1 = \chi w_{\chi,1} + \eta w_{\eta,1} + \tau w_{\tau,1},\;\; \theta_4 = w_{1,4}F_1(\theta_1) + w_{2,4}F_2(\theta_2) + w_{3,4}F_3(\theta_3),\\
&\theta_2 = \chi w_{\chi,2} + \eta w_{\eta,2} + \tau w_{\tau,2},\;\; \theta_5 = w_{1,5}F_1(\theta_1) + w_{2,5}F_2(\theta_2) + w_{3,5}F_3(\theta_3),\\
&\theta_3 = \chi w_{\chi,3} + \eta w_{\eta,3} + \tau w_{\tau,3},\;\; \theta_6 = w_{1,6}F_1(\theta_1) + w_{2,6}F_2(\theta_2) + w_{3,6}F_3(\theta_3).
\end{aligned}
\tag{2.16}
$$

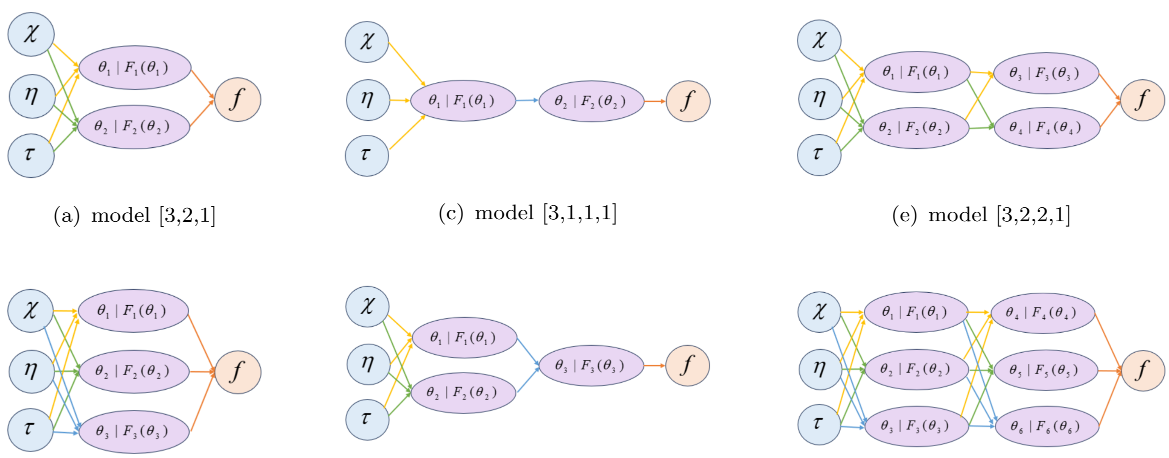

(a) model [3,2,1] (c) model [3,1,1,1] (e) model [3,2,2,1]

(b) model [3,3,1] (d) model [3,2,1,1] (f) model [3,3,3,1]

Figure 2. Six neural network models.

3. Novel exact solutions for equation (1.1)

In this section, we constructing various test functions based on six neural network models in Figure 2 to solve the reduction equation (2.6) and (2.10).

3.1. Solutions based on the reduction equation (2.6)

3.1.1. Case 1

Giving the formula (2.11) of **model [3,2,1]**, when supposing $F_1(\theta_1) = \theta_1$, $F_2(\theta_2) = \csc(\theta_2)$, the test function is given by

$$f = w_{1,f}(\theta_1) + w_{2,f}\csc(\theta_2) + b_3. \tag{3.1}$$

Substituting (3.1) into the Eq. (2.6) and solving it by mathematical software in accordance with the framework and main steps illustrated in Subsection 2.1, we obtain 4 sets of solutions, one of which is presented as

$$\left\{\begin{array}{l} w_{\chi,1} = -\dfrac{2w_{1,f}w_{\chi,2}^2 w_{\eta,1} + 2w_{1,f}w_{\chi,2}^2 w_{\tau,1} - 5w_{\chi,2}^2 - 2w_{\chi,2}w_{\tau,2} - 3w_{\tau,2}^2}{2w_{1,f}w_{\chi,2}^2}, w_{\chi,2} = w_{\chi,2}, \\ w_{\eta,1} = w_{\eta,1}, w_{\eta,2} = -w_{\chi,2} - w_{\tau,2}, w_{\tau,1} = w_{\tau,1}, w_{\tau,2} = w_{\tau,2}, w_{1,f} = w_{1,f}, w_{2,f} = w_{2,f} \end{array}\right\}. \tag{3.2}$$

Substituting (3.2) into (3.1) yields

$$\begin{aligned} f = {} & w_{1,f}\Bigg(-\frac{\chi(2w_{1,f}w_{\chi,2}^2 w_{\eta,1} + 2w_{1,f}w_{\chi,2}^2 w_{\tau,1} - 5w_{\chi,2}^2 - 2w_{\chi,2}w_{\tau,2} - 3w_{\tau,2}^2)}{2w_{1,f}w_{\chi,2}^2} \\ & + \eta w_{\eta,1} + \tau w_{\tau,1}\Bigg) + w_{2,f}\csc\Big(\chi w_{\chi,2} + \eta(-w_{\chi,2} - w_{\tau,2}) + \tau w_{\tau,2}\Big) + b_3. \end{aligned} \tag{3.3}$$

Substituting (3.3) into (2.5), one obtains group-invariant solution u_1:

$$\begin{aligned} u_1 = {} & w_{1,f}\Bigg(\frac{(-z+x)(5w_{\chi,2}^2 + 2w_{\chi,2}w_{\tau,2} + 3w_{\tau,2}^2)}{2w_{1,f}w_{\chi,2}^2} - (-z+x)(w_{\eta,1} + w_{\tau,1}) \\ & + (-z+y)w_{\eta,1} + (-z+t)w_{\tau,1}\Bigg) \\ & + w_{2,f}\csc\Big((-z+x)w_{\chi,2} + (-z+y)(-w_{\chi,2} - w_{\tau,2}) + (-z+t)w_{\tau,2}\Big) + z + b_3. \end{aligned} \tag{3.4}$$

Selecting appropriate parameter values, the profiles of u_1 are shown in Figure 3.

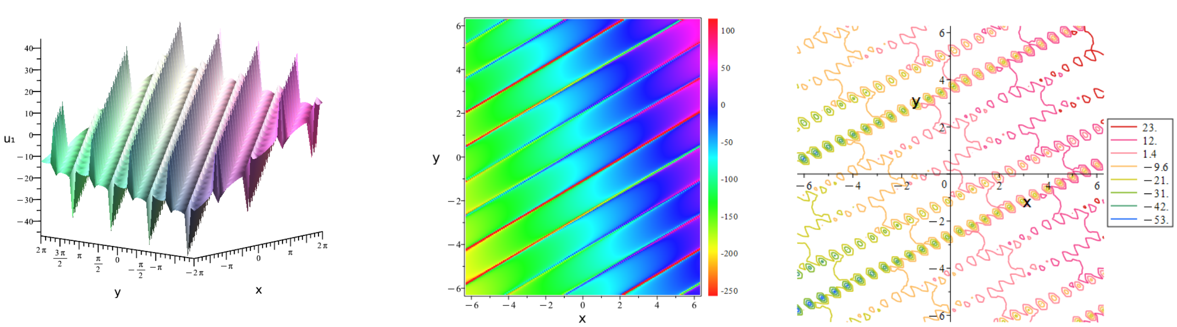

(a) 3D plot (b) density plot (c) contour plot

Figure 3. The profiles of solution u_1, with $z = 1, t = 1, b_3 = 2, w_{1,f} = 1, w_{2,f} = 1, w_{\eta,1} = 1, w_{\tau,1} = 1, w_{\chi,2} = 1, w_{\tau,2} = 1$.

3.1.2. Case 2

Giving the formula (2.12) of **model [3,3,1]**, when supposing $F_1(\theta_1) = \theta_1$, $F_2(\theta_2) = \tan(\theta_2)$, $F_3(\theta_3) = \mathrm{JacobiCN}(\theta_3, \frac{3}{5})$, the test functions is given by

$$f = w_{1,f}(\theta_1) + w_{2,f}\tan(\theta_2) + w_{3,f}\,\mathrm{JacobiCN}(\theta_3, \frac{3}{5}) + b_4. \tag{3.5}$$

Substituting (3.5) into the Eq. (2.6) yields 22 sets of solutions, one of which is presented as

$$\left\{\begin{aligned} & w_{\chi,1} = -\frac{2w_{1,f}w_{\chi,3}^2 w_{\eta,1} + 2w_{1,f}w_{\chi,3}^2 w_{\tau,1} - 5w_{\chi,3}^2 - 2w_{\chi,3}w_{\tau,3} - 3w_{\tau,3}^2}{2w_{1,f}w_{\chi,3}^2}, \\ & w_{\chi,2} = w_{\chi,2}, w_{\chi,3} = w_{\chi,3}, w_{\eta,1} = w_{\eta,1}, w_{\eta,2} = \frac{-w_{\chi,2}(w_{\chi,3} - 3w_{\tau,3})}{3w_{\chi,3}}, \\ & w_{\eta,3} = -w_{\chi,3} - w_{\tau,3}, w_{\tau,1} = w_{\tau,1}, w_{\tau,2} = \frac{-w_{\chi,2}(2w_{\chi,3} + 3w_{\tau,3})}{3w_{\chi,3}}, \\ & w_{\tau,3} = w_{\tau,3}, w_{1,f} = w_{1,f}, w_{2,f} = w_{2,f}, w_{3,f} = w_{3,f} \end{aligned}\right\}. \tag{3.6}$$

Substituting (3.6) into (3.5) yields

$$\begin{aligned} f = \; & w_{1,f}\left(\frac{\chi(5w_{\chi,3}^2 + 2w_{\chi,3}w_{\tau,3} + 3w_{\tau,3}^2)}{2w_{1,f}w_{\chi,3}^2} - \chi(w_{\eta,1} + w_{\tau,1}) + \eta w_{\eta,1} + \tau w_{\tau,1}\right) \\ & + w_{2,f}\tan\left(\chi w_{\chi,2} - \frac{\eta w_{\chi,2}(w_{\chi,3} - 3w_{\tau,3})}{3w_{\chi,3}} - \frac{\tau w_{\chi,2}(2w_{\chi,3} + 3w_{\tau,3})}{3w_{\chi,3}}\right) \\ & + w_{3,f}\,\mathrm{JacobiCN}\left(\chi w_{\chi,3} + \eta\big(-w_{\tau,3} - w_{\chi,3}\big) + \tau w_{\tau,3}, \frac{3}{5}\right) + b_4. \end{aligned} \tag{3.7}$$

Then substituting (3.7) into (2.5), one obtains group-invariant solution u_2:

$$\begin{aligned} u_2 = \; & w_{1,f}\left(\frac{(-z+x)(5w_{\chi,3}^2 + 2w_{\chi,3}w_{\tau,3} + 3w_{\tau,3}^2)}{2w_{1,f}w_{\chi,3}^2} - (-z+x)(w_{\eta,1} + w_{\tau,1})\right. \\ & \left. + (-z+y)w_{\eta,1} + (-z+t)w_{\tau,1}\right) + w_{2,f}\tan\left(-\frac{(-z+y)w_{\chi,2}(w_{\chi,3} - 3w_{\tau,3})}{3w_{\chi,3}}\right. \\ & \left. - \frac{(-z+t)w_{\chi,2}(2w_{\chi,3} + 3w_{\tau,3})}{3w_{\chi,3}} + (-z+x)w_{\chi,2}\right) + w_{3,f}\,\mathrm{JacobiCN}\left((-z+x)w_{\chi,3}\right. \\ & \left. + (-z+y)(-w_{\chi,3} - w_{\tau,3}) + (-z+t)w_{\tau,3}, \frac{3}{5}\right) + z + b_4. \end{aligned} \tag{3.8}$$

Selecting appropriate parameter values, the profiles of u_2 are graphically demonstrated in Figure 4.

3.1.3. Case 3

Giving the formula (2.13) of **model [3,1,1,1]**, when suppose $F_1(\theta_1) = (\theta_1)^n (n \in R)$, $F_2(\theta_2) = (\theta_2)^{-1}$, $b_3 = 0$, the test function is given as

$$f = w_{2,f}\big(w_{1,2}(\theta_1)^n + b_2\big)^{-1}. \tag{3.9}$$

Substituting (3.9) into the Eq. (2.6) yields 5 sets of solutions, one of which is presented as

$$\left\{\begin{aligned} & n = n, w_{1,2} = w_{1,2}, w_{2,f} = w_{2,f}, w_{\chi,1} = \mathrm{RootOf}(A)w_{\tau,1}, \\ & w_{\eta,1} = -\mathrm{RootOf}(A)w_{\tau,1} - w_{\tau,1}, w_{\tau,1} = w_{\tau,1} \end{aligned}\right\}, \tag{3.10}$$

where $A = 5Z^2 + 2Z + 3$, then $\mathrm{RootOf}(A) = -\frac{1}{5} \pm \frac{\sqrt{14}i}{5}$. Substituting (3.10) into (3.9) yields

$$f = \frac{w_{2,f}}{w_{1,2}\Big(\chi\mathrm{RootOf}(A)w_{\tau,1} + \eta(-\mathrm{RootOf}(A) - 1)w_{\tau,1} + \tau w_{\tau,1}\Big)^n + b_2}. \tag{3.11}$$

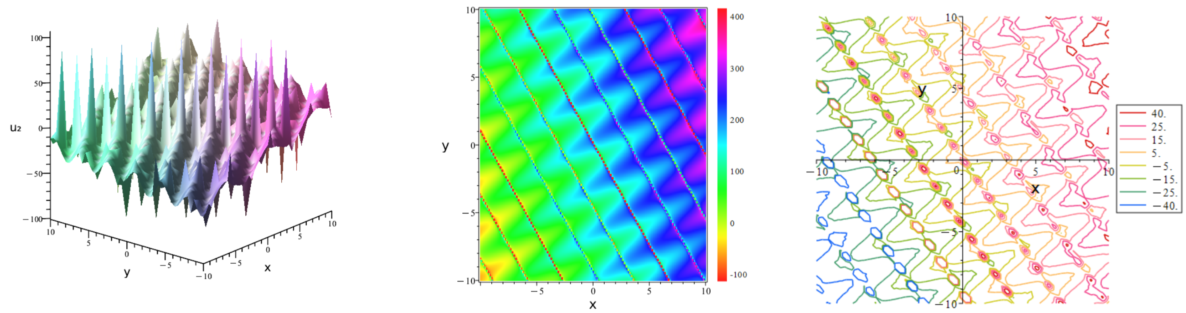

(a) 3D plot (b) density plot (c) contour plot

Figure 4. The profiles of solution u_2, with $z = 1, t = 1, b_4 = 2, w_{1,f} = 1, w_{2,f} = 1, w_{3,f} = 10, w_{\eta,1} = 1, w_{\tau,1} = 1, w_{\chi,2} = 1, w_{\chi,3} = 1, w_{\tau,3} = 1$.

Substituting (3.11) into (2.5) and choosing $\mathrm{RootOf}(A) = -\frac{1}{5} + \frac{\sqrt{14}i}{5}$, one obtains group-invariant solution u_3:

$$u_3 = \frac{w_{2,f}}{w_{1,2}\Big((-z+x)(-\frac{1}{5}+\frac{\sqrt{14}i}{5})w_{\tau,1} + (-z+y)\big(-\frac{4}{5}-\frac{\sqrt{14}i}{5}\big)w_{\tau,1} + (-z+t)w_{\tau,1}\Big)^n + b_2} + z. \tag{3.12}$$

Selecting other parameter values appropriately, the profiles of u_3 are graphically demonstrated in Figure 5.

3.1.4. Case 4

Giving the formula (2.14) of **model [3,2,1,1]**, when suppose $F_1(\theta_1) = \cosh(\theta_1)$, $F_2(\theta_2) = \cos(\theta_2)$, $F_3(\theta_3) = (\theta_3)^{-1}$, $b_4 = 0$, the test function is

$$f = w_{3,f}\Big(w_{1,3}\cosh(\theta_1) + w_{2,3}\cos(\theta_2) + b_3\Big)^{-1}. \tag{3.13}$$

Substituting (3.13) into the Eq. (2.6) yields 10 sets of solutions, one of which is presented as

$$\left\{\begin{aligned} & w_{1,3} = w_{1,3}, w_{2,3} = w_{2,3}, w_{3,f} = w_{3,f}, w_{\chi,1} = w_{\tau,1}\Big(\frac{2\mathrm{RootOf}(B)+3}{4\mathrm{RootOf}(B)-1}\Big), \\ & w_{\chi,2} = \mathrm{RootOf}(B)w_{\eta,2}, w_{\eta,1} = -2w_{\tau,1}\Big(\frac{3\mathrm{RootOf}(B)+1}{4\mathrm{RootOf}(B)-1}\Big), \\ & w_{\eta,2} = w_{\eta,2}, w_{\tau,1} = w_{\tau,1}, w_{\tau,2} = -\mathrm{RootOf}(B)w_{\eta,2} - w_{\eta,2} \end{aligned}\right\}, \tag{3.14}$$

where $B = 6Z^2 + 4Z + 3$, then $\mathrm{RootOf}(B) = -\frac{1}{3} \pm \frac{\sqrt{14}i}{6}$. Substituting (3.14) into (3.13) yields

$$f = \frac{w_{3,f}}{w_{1,3}\cosh\big(\chi M - 2\eta N + \tau w_{\tau,1}\big) + w_{2,3}\cos\big(\chi K + \eta w_{\eta,2} - \tau(K + w_{\eta,2})\big) + b_3}, \tag{3.15}$$

where

$$M = \Big(\frac{2\mathrm{RootOf}(B)+3}{4\mathrm{RootOf}(B)-1}\Big)w_{\tau,1}, \quad N = \Big(\frac{3\mathrm{RootOf}(B)+1}{4\mathrm{RootOf}(B)-1}\Big)w_{\tau,1}, \quad K = \mathrm{RootOf}(B)w_{\eta,2}.$$

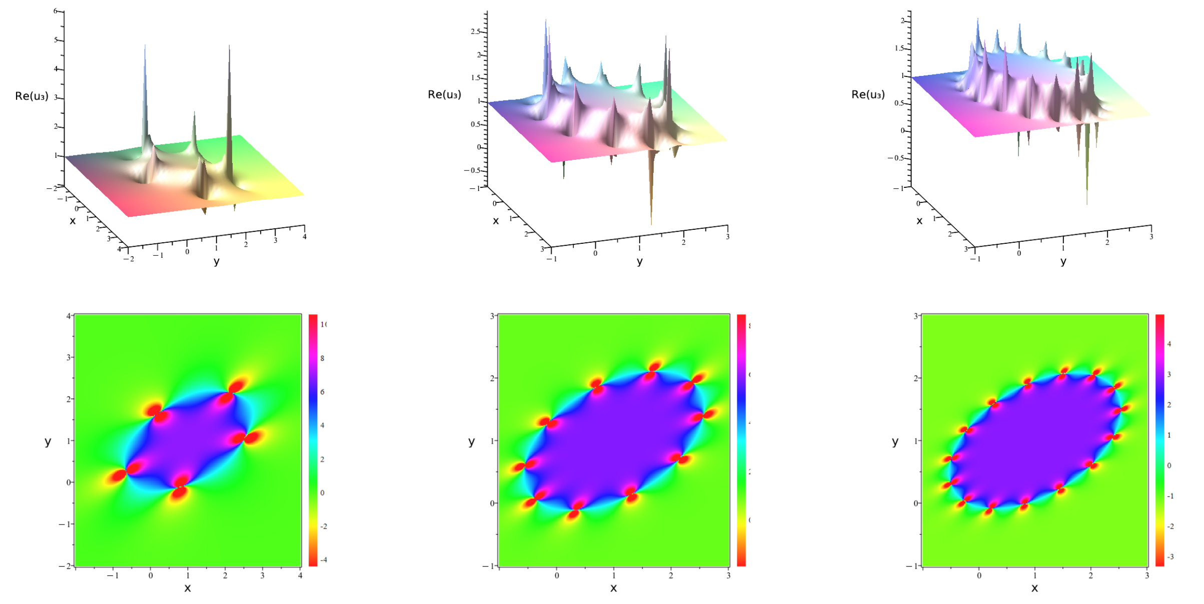

(a) n=5 (b) n=10 (c) n=15

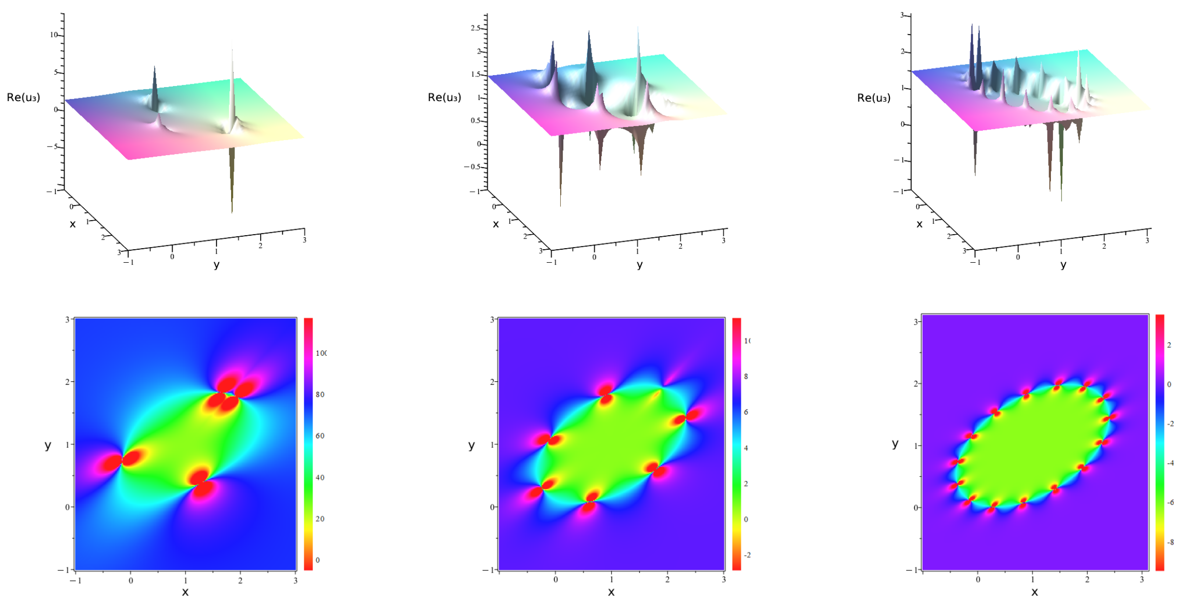

(d) $n = -\sqrt{10}$ (e) $n = -\frac{34}{5}$ (f) n=-15

Figure 5. The real part profiles of solution u_3 with respect to parameter n, with $t = 1, z = 1, b_2 = 2, w_{2,f} = 1, w_{1,2} = 1, w_{\tau,1} = 1$.

Substituting (3.15) into (2.5) and choosing RootOf$(B) = -\frac{1}{3} + \frac{\sqrt{14}i}{6}$, one obtains group invariant solution u_4:

$$u_4 = \frac{w_{3,f}}{w_{1,3}\cosh(P) + w_{2,3}\cos(Q) + b_3} + z, \tag{3.16}$$

where

$$
\begin{aligned}
P = &\quad (-z+x)\Big(\frac{\frac{7}{3}+\frac{\sqrt{14}}{3}i}{-\frac{7}{3}+\frac{2\sqrt{14}i}{3}}\Big)w_{\tau,1} - (-z+y)\Big(\frac{\sqrt{14}i}{-\frac{7}{3}+\frac{2\sqrt{14}i}{3}}\Big)w_{\tau,1} + (-z+t)w_{\tau,1},\\
Q = &\quad (-z+x)\Big(-\frac{1}{3}+\frac{\sqrt{14}i}{6}\Big)w_{\eta,2} + (-z+y)w_{\eta,2} + (-z+t)\Big(-(-\frac{1}{3}+\frac{\sqrt{14}i}{6})w_{\eta,2} - w_{\eta,2}\Big).
\end{aligned}
$$

Selecting other parameters appropriately, the dynamic characteristics of u_4 are intuitively illustrated in Figure 6.

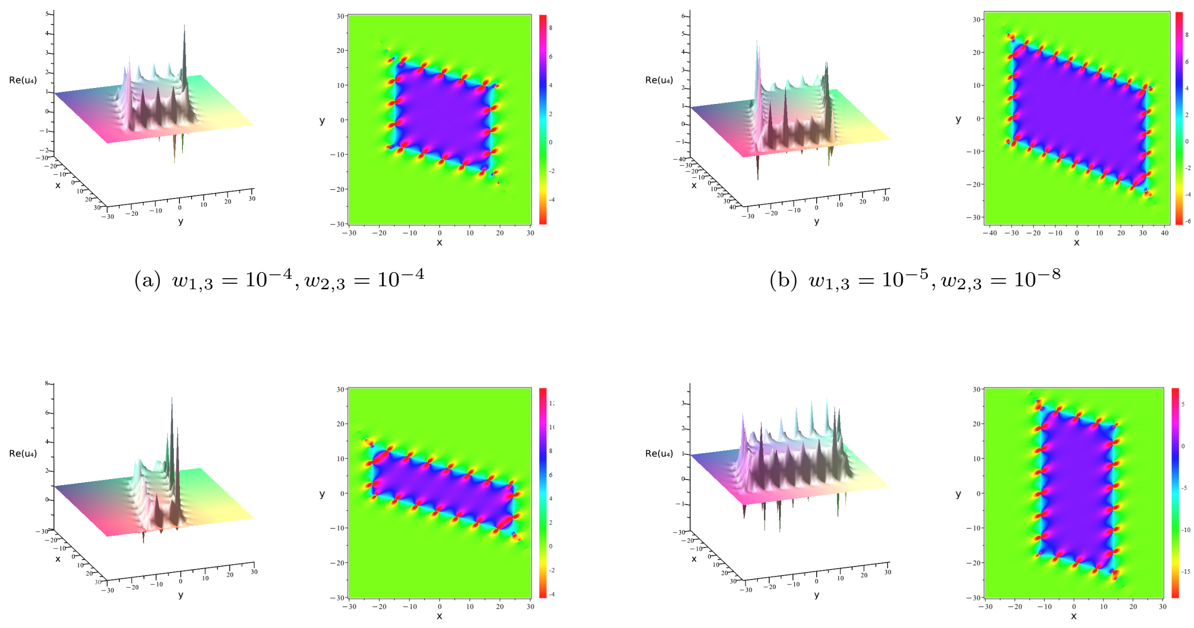

(a) $w_{1,3}=10^{-4}, w_{2,3}=10^{-4}$

(b) $w_{1,3}=10^{-5}, w_{2,3}=10^{-8}$

(c) $w_{1,3}=10^{-2}, w_{2,3}=10^{-6}$

(d) $w_{1,3}=10^{-7}, w_{2,3}=10^{-3}$

Figure 6. The real part evolution plots of solution u_4 with respect to parameters $w_{1,3}$ and $w_{2,3}$, with $z=1, t=1, b_3=1, w_{3,f}=1, w_{\tau,1}=1, w_{\eta,2}=1$.

3.1.5. Case 5

Giving the formula (2.15) of **model [3,2,2,1]**, when suppose $F_1(\theta_1)=\theta_1$, $F_2(\theta_2)=(\theta_2)^2$, $F_3(\theta_3)=\theta_3$, $F_4(\theta_4)=\text{JacobiCN}(\theta_4,\frac{3}{5})$, $b_3=0$, $b_4=0$, the test function is

$$
f = w_{3,f}\Big(w_{1,3}(\theta_1)+w_{2,3}(\theta_2)^2\Big) + w_{4,f}\,\text{JacobiCN}\left(w_{1,4}(\theta_1)+w_{2,4}(\theta_2)^2, \frac{2}{5}\right) + b_5. \tag{3.17}
$$

Substituting (3.17) into the Eq. (2.6) yields 20 sets of solutions, one of which is presented as

$$
\left\{
\begin{aligned}
&w_{1,3}=w_{1,3}, w_{1,4}=0, w_{2,3}=w_{2,3}, w_{2,4}=w_{2,4}, w_{3,f}=w_{3,f}, w_{4,f}=w_{4,f},\\
&w_{\chi,1}=-\frac{2w_{1,3}w_{3,f}w_{\chi,2}^2w_{\eta,1}+2w_{1,3}w_{3,f}w_{\chi,2}^2w_{\tau,1}-5w_{\chi,2}^2-2w_{\chi,2}w_{\tau,2}-3w_{\tau,2}^2}{2w_{1,3}w_{3,f}w_{\chi,2}^2},\\
&w_{\chi,2}=w_{\chi,2}, w_{\eta,1}=w_{\eta,1}, w_{\eta,2}=-w_{\tau,2}-w_{\chi,2}, w_{\tau,1}=w_{\tau,1}, w_{\tau,2}=w_{\tau,2}
\end{aligned}
\right\}. \tag{3.18}
$$

Substituting (3.18) into (3.17) yields

$$
\begin{aligned}
f = \ & w_{3,f}\Bigg(w_{1,3}\Big(\frac{\chi(5w_{\chi,2}^2 + 2w_{\chi,2}w_{\tau,2} + 3w_{\tau,2}^2)}{2w_{1,3}w_{3,f}w_{\chi,2}^2} - \chi(w_{\eta,1} + w_{\tau,1}) + \eta w_{\eta,1} + \tau w_{\tau,1}\Big) \\
& + w_{2,3}\Big(\chi w_{\chi,2} + \eta(-w_{\tau,2} - w_{\chi,2}) + \tau w_{\tau,2}\Big)^2\Bigg) \\
& + w_{4,f}\,\mathrm{JacobiCN}\left(w_{2,4}\Big(\chi w_{\chi,2} + \eta(-w_{\tau,2} - w_{\chi,2}) + \tau w_{\tau,2}\Big)^2, \frac{3}{5}\right) + b_5.
\end{aligned} \tag{3.19}
$$

Substituting (3.19) into (2.5) obtains group-invariant solution u_5:

$$
\begin{aligned}
u_5 = \ & w_{3,f}\Bigg(w_{1,3}\Big(\frac{(-z+x)(5w_{\chi,2}^2 + 2w_{\chi,2}w_{\tau,2} + 3w_{\tau,2}^2)}{2w_{1,3}w_{3,f}w_{\chi,2}^2} - (-z+x)(w_{\eta,1} + w_{\tau,1}) + (-z+y)w_{\eta,1} \\
& + (-z+t)w_{\tau,1}\Big) + w_{2,3}\Big((-z+x)w_{\chi,2} + (-z+y)(-w_{\tau,2} - w_{\chi,2}) + (-z+t)w_{\tau,2}\Big)^2\Bigg) \\
& + w_{4,f}\,\mathrm{JacobiCN}\left(w_{2,4}\Big((-z+x)w_{\chi,2} + (-z+y)(-w_{\tau,2} - w_{\chi,2}) + (-z+t)w_{\tau,2}\Big)^2, \frac{3}{5}\right) \\
& + z + b_5.
\end{aligned} \tag{3.20}
$$

Selecting appropriate parameter values, the characteristics of u_5 are vividly depicted in Figure 7.

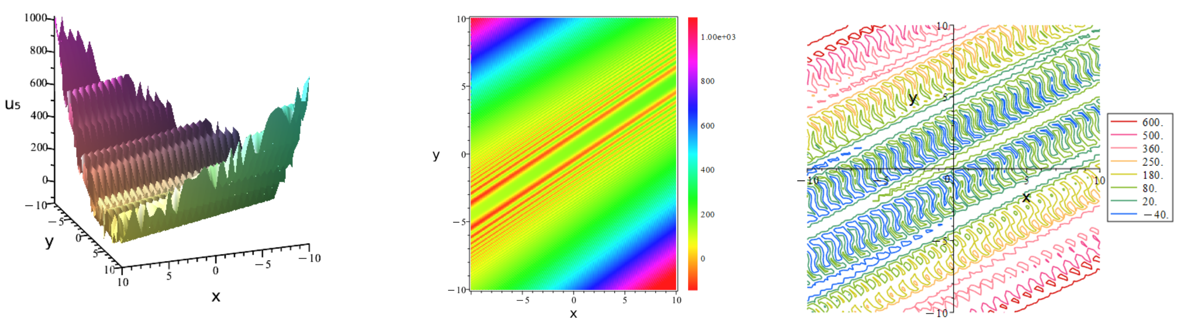

(a) 3D plot (b) density plot (c) contour plot

Figure 7. The profiles of solution u_5, with $z = 1, t = 1, b_5 = 2, w_{3,f} = 1, w_{4,f} = 100, w_{1,3} = 1, w_{2,3} = 1, w_{2,4} = 1, w_{\eta,1} = 1, w_{\tau,1} = 1, w_{\chi,2} = 1, w_{\tau,2} = 1$.

3.1.6. Case 6

Giving the formula (2.16) of **model [3,3,3,1]**, we set the weight coefficients of the neural network model with appropriate values for simplicity: $w_{1,4} = 1$, $w_{2,4} = 1$, $w_{3,4} = 1$, $w_{1,5} = 1$, $w_{2,5} = 1$, $w_{3,5} = 1$, $w_{1,6} = 1$, $w_{2,6} = 1$, $w_{3,6} = 1$. When suppose activation function $F_1(\theta_1) = \theta_1$, $F_2(\theta_2) = (\theta_2)^2$, $F_3(\theta_3) = (\theta_3)^3$, $F_4(\theta_4) = \theta_4$, $F_5(\theta_5) = \theta_5$, $F_6(\theta_6) = \theta_6$, the test functions is given as:

$$
f = w_{4,f}(\theta_1 + \theta_2^2 + \theta_3^3) + w_{5,f}(\theta_1 + \theta_2^2 + \theta_3^3) + w_{6,f}(\theta_1 + \theta_2^2 + \theta_3^3) + b_7. \tag{3.21}
$$

Substituting (3.21) into the Eq. (2.6) yields 9 sets of solutions, one of which is presented as

$$\left\{\begin{array}{l} w_{\chi,1} = -\dfrac{2w_{4,f}w_{\eta,1} + 2w_{4,f}w_{\tau,1} + 2w_{5,f}w_{\eta,1} + 2w_{5,f}w_{\tau,1} + 2w_{6,f}w_{\eta,1} + 2w_{6,f}w_{\tau,1} - 5}{2\left(w_{4,f} + w_{5,f} + w_{6,f}\right)}, \\ w_{\chi,2} = -3\, w_{\eta,2}, w_{\chi,3} = w_{\chi,3}, w_{\eta,1} = w_{\eta,1}, w_{\eta,2} = w_{\eta,2}, w_{\eta,3} = -w_{\chi,3}, \\ w_{\tau,1} = w_{\tau,1}, w_{\tau,2} = 2\, w_{\eta,2}, w_{\tau,3} = 0, w_{4,f} = w_{4,f}, w_{5,f} = w_{5,f}, w_{6,f} = w_{6,f} \end{array}\right\}. \tag{3.22}$$

Substituting (3.22) into (3.21) yields

$$\begin{aligned} f =\ & \left(w_{4,f} + w_{5,f} + w_{6,f}\right)\Big(\chi\, C + \eta\, w_{\eta,1} + \tau\, w_{\tau,1} + \left(-3\chi w_{\eta,2} + \eta w_{\eta,2} + 2\tau w_{\eta,2}\right)^2 \\ & + \left(\chi w_{\chi,3} - \eta w_{\chi,3}\right)^3\Big) + b_7, \end{aligned} \tag{3.23}$$

where

$$C = -\frac{2w_{4,f}w_{\eta,1} + 2w_{4,f}w_{\tau,1} + 2w_{5,f}w_{\eta,1} + 2w_{5,f}w_{\tau,1} + 2w_{6,f}w_{\eta,1} + 2w_{6,f}w_{\tau,1} - 5}{2(w_{4,f} + w_{5,f} + w_{6,f})}.$$

Substituting (3.23) into (2.5) obtains group-invariant solution u_6:

$$\begin{aligned} u_6 =\ & \left(w_{4,f} + w_{5,f} + w_{6,f}\right)\Big((-z + x)\, C + (-z + y)\, w_{\eta,1} + (-z + t)\, w_{\tau,1} + \big(-3(-z + x)w_{\eta,2} \\ & + (-z + y)w_{\eta,2} + 2(-z + t)w_{\eta,2}\big)^2 + \left((-z + x)w_{\chi,3} - (-z + y)w_{\chi,3}\right)^3\Big) + z + b_7. \end{aligned} \tag{3.24}$$

Selecting appropriate parameter values, the properties of u_6 are graphically demonstrated in Figure 8.

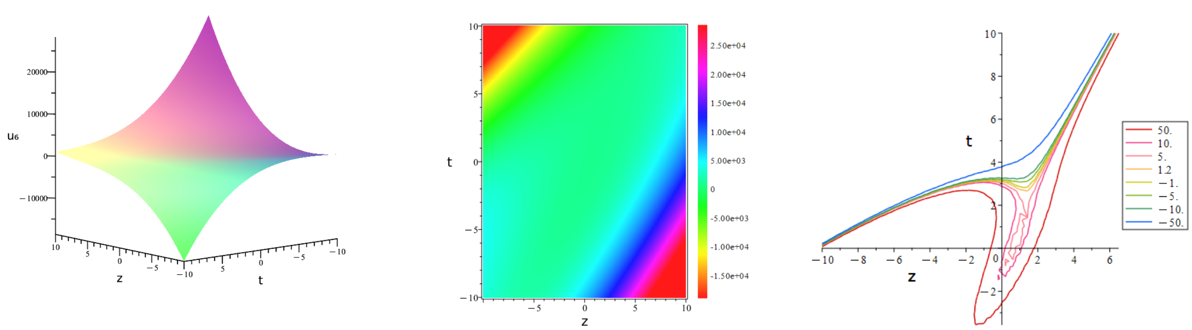

(a) 3D plot (b) density plot (c) contour plot

Figure 8. The profiles of solution u_6, with $z = 1, t = 1, b_7 = 2, w_{4,f} = 1, w_{5,f} = 1, w_{6,f} = 1, w_{\eta,1} = 1, w_{\tau,1} = 1, w_{\chi,3} = 1, w_{\eta,2} = 1$.

3.2. Solutions based on the reduction equation (2.10)

3.2.1. Case 1

According to the formula (2.11) of **model [3,2,1]**, when supposing $F_1(\theta_1) = \mathrm{sech}(\theta_1)$, $F_2(\theta_2) = \sin(\theta_2)$, the test function is given as

$$f = w_{1,f}\, \mathrm{sech}(\theta_1) + w_{2,f} \sin(\theta_2) + b_3. \tag{3.25}$$

Substituting (3.25) into the Eq. (2.10) derives 12 sets of solutions, one of which is expressed as

$$\left\{\begin{matrix} w_{1,f}=w_{1,f}, w_{2,f}=w_{2,f}, w_{\chi,1}=-\dfrac{3w_{\eta,1}}{4}, w_{\chi,2}=-\dfrac{3w_{\eta,2}}{4}, \\ w_{\eta,1}=w_{\eta,1}, w_{\eta,2}=w_{\eta,2}, w_{\tau,1}=0, w_{\tau,2}=0 \end{matrix}\right\}. \tag{3.26}$$

Substituting (3.26) into (3.25) yields

$$f=w_{1,f}\operatorname{sech}\Big(-\frac{3}{4}\chi w_{\eta,1}+\eta w_{\eta,1}\Big)+w_{2,f}\sin\Big(-\frac{3}{4}\chi w_{\eta,2}+\eta w_{\eta,2}\Big)+b_3. \tag{3.27}$$

Substituting (3.27) into (2.9), one obtains group-invariant solution u_7:

$$\begin{aligned} u_7=\ & w_{1,f}\operatorname{sech}\Big(\frac{3w_{\eta,1}}{4}(-\frac{t^2}{2}+x)-(-t+y)w_{\eta,1}\Big) \\ & -w_{2,f}\sin\Big(\frac{3w_{\eta,2}}{4}(-\frac{t^2}{2}+x)-(-t+y)w_{\eta,2}\Big)+t^2-2tz+b_3. \end{aligned} \tag{3.28}$$

Choosing appropriate parameters, the profiles of u_7 are graphically demonstrated in Figure 9.

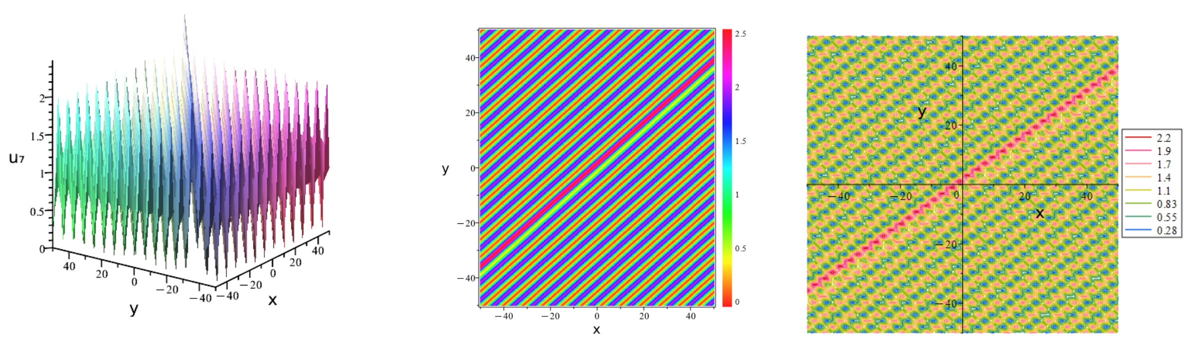

(a) 3D plot (b) density plot (c) contour plot

Figure 9. The profiles of solution u_7, with $z=1, t=1, b_3=2, w_{1,f}=1, w_{2,f}=1, w_{\eta,1}=1, w_{\eta,2}=1$.

3.2.2. Case 2

Following the formula (2.12) of **model [3,3,1]**, when supposing $F_1(\theta_1)=\theta_1$, $F_2(\theta_2)=\cot(\theta_2)$, $F_3(\theta_3)=\text{JacobiCN}(\theta_3,\frac{3}{5})$, the test functions are given by

$$f=w_{1,f}(\theta_1)+w_{2,f}\cot(\theta_2)+w_{3,f}\,\text{JacobiCN}(\theta_3,\frac{3}{5})+b_4. \tag{3.29}$$

Substituting (3.29) into the Eq. (2.10) derives 29 sets of solutions, one of which is expressed as

$$\left\{\begin{matrix} w_{1,f}=w_{1,f}, w_{2,f}=w_{2,f}, w_{3,f}=w_{3,f}, w_{\chi,1}=w_{\chi,1}, w_{\chi,2}=w_{\chi,2}, w_{\chi,3}=w_{\chi,3}, w_{\eta,1}=w_{\eta,1}, \\ w_{\eta,2}=\dfrac{-w_{\chi,2}(4w_{\chi,3}+3w_{\eta,3})}{3w_{\chi,3}}, w_{\eta,3}=w_{\eta,3}, w_{\tau,1}=\dfrac{-w_{\eta,3}(4w_{\chi,3}+3w_{\eta,3})}{2w_{1,f}w_{\chi,3}^2}, w_{\tau,2}=0, w_{\tau,3}=0 \end{matrix}\right\}. \tag{3.30}$$

Substituting (3.30) into (3.29) yields

$$
\begin{aligned}
f =\ & w_{1,f}\left(\chi w_{\chi,1}+\eta w_{\eta,1}-\frac{\tau w_{\eta,3}(4w_{\chi,3}+3w_{\eta,3})}{2w_{1,f}w_{\chi,3}^2}\right)+w_{2,f}\cot\left(\chi w_{\chi,2}-\frac{\eta w_{\chi,2}(4w_{\chi,3}+3w_{\eta,3})}{3w_{\chi,3}}\right)\\
&+w_{3,f}\mathrm{JacobiCN}\left(\chi w_{\chi,3}+\eta w_{\eta,3},\frac{3}{5}\right)+b_4.
\end{aligned}
\tag{3.31}
$$

Substituting (3.31) into (2.9), one obtains group-invariant solutions u_8:

$$
\begin{aligned}
u_8 =\ & w_{1,f}\left(\left(-\frac{t^2}{2}+x\right)w_{\chi,1}+(-t+y)w_{\eta,1}-\frac{(-t+z)w_{\eta,3}(4w_{\chi,3}+3w_{\eta,3})}{2w_{1,f}w_{\chi,3}^2}\right)\\
&+w_{2,f}\cot\left(\left(-\frac{t^2}{2}+x\right)w_{\chi,2}-\frac{(-t+y)w_{\chi,2}(4w_{\chi,3}+3w_{\eta,3})}{3w_{\chi,3}}\right)\\
&+w_{3,f}\mathrm{JacobiCN}\left(\left(-\frac{t^2}{2}+x\right)w_{\chi,3}+(-t+y)w_{\eta,3},\frac{3}{5}\right)+t^2-2tz+b_4.
\end{aligned}
\tag{3.32}
$$

Selecting appropriate parameters, the profiles of u_8 are graphically demonstrated in Figure 10.

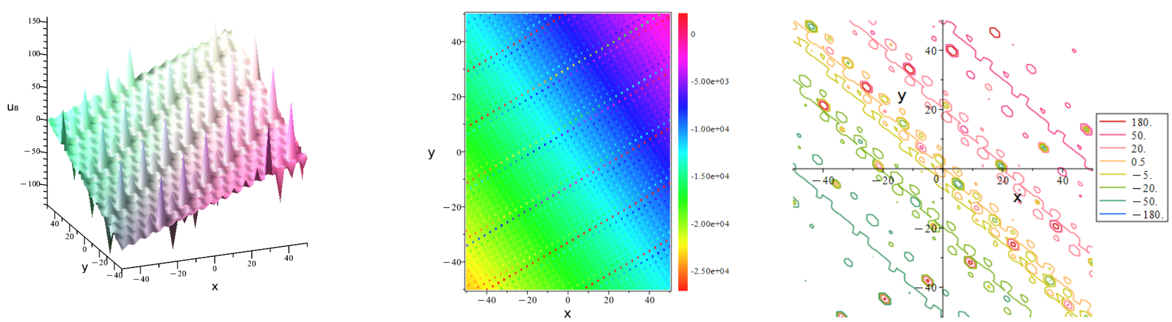

(a) 3D plot (b) density plot (c) contour plot

Figure 10. The profiles of solution u_8, with $z=1, t=1, b_4=2, w_{1,f}=1, w_{2,f}=1, w_{3,f}=1, w_{\chi,1}=1, w_{\chi,2}=1, w_{\chi,3}=1, w_{\eta,1}=1, w_{\eta,3}=1$.

3.2.3. Case 3

Following the formula (2.13) of **model [3,1,1,1]**, when suppose $F_1(\theta_1)=\cos(\theta_1)$, $F_2(\theta_2)=\exp(\theta_2)$, the test function is given by

$$f=w_{2,f}\exp\big(w_{1,2}\cos(\theta_1)\big)+b_3. \tag{3.33}$$

Substituting (3.33) into the Eq. (2.10) derives 5 sets of solutions, one of which is expressed as

$$\left\{w_{1,2}=w_{1,2}, w_{2,f}=w_{2,f}, w_{\chi,1}=-\frac{3w_{\eta,1}}{4}, w_{\eta,1}=w_{\eta,1}, w_{\tau,1}=0\right\}. \tag{3.34}$$

Substituting (3.34) into (3.33) yields

$$f=w_{2,f}\exp\Big(w_{1,2}\cos\big(-\frac{3w_{\eta,1}}{4}\chi+\eta w_{\eta,1}\big)\Big)+b_3. \tag{3.35}$$

Substituting (3.35) into (2.9), one obtains group-invariant solution u_9:

$$u_9 = w_{2,f} \exp\Big(w_{1,2} \cos\big(- \frac{3w_{\eta,1}}{4}(-\frac{t^2}{2} + x) + (-t + y)w_{\eta,1}\big)\Big) + t^2 - 2tz + b_3. \tag{3.36}$$

Selecting appropriate parameters, the profiles of u_9 are graphically demonstrated in Figure 11.

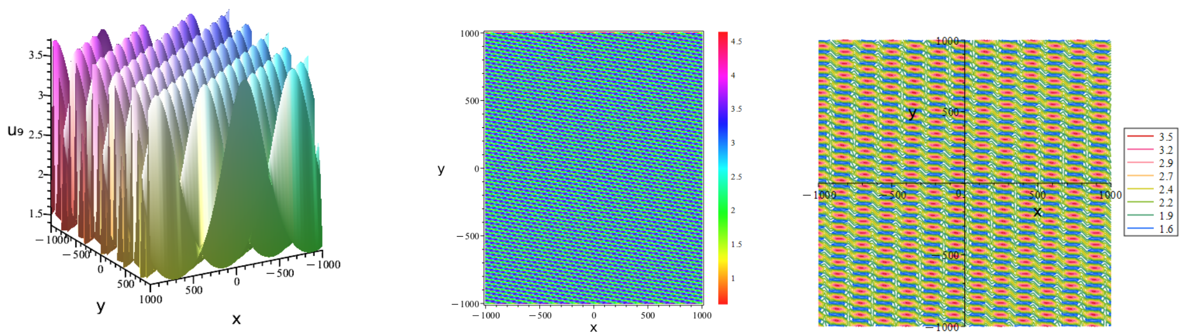

(a) 3D plot (b) density plot (c) contour plot

Figure 11. The profiles of solution u_9 (3.36), with $z = 1, t = 1, b_3 = 2, w_{2,f} = 1, w_{1,2} = 1, w_{\eta,1} = 1$.

3.2.4. Case 4

Following the formula (2.14) of **model [3,2,1,1]**, when suppose $F_1(\theta_1) = \sec(\theta_1)$, $F_2(\theta_2) = \operatorname{arccot}(\theta_2)$, $F_3(\theta_3) = (\theta_3)^2$, the test function is

$$f = w_{3,f}\Big(w_{1,3}\sec(\theta_1) + w_{2,3}\operatorname{arccot}(\theta_2)\Big)^2 + b_4. \tag{3.37}$$

Substituting (3.37) into the Eq. (2.10) derives 11 sets of solutions, one of which is expressed as

$$\left\{\begin{matrix} w_{1,3} = w_{1,3}, w_{2,3} = w_{2,3}, w_{3,f} = w_{3,f}, w_{\chi,1} = -\dfrac{3w_{\eta,1}}{4}, w_{\chi,2} = -\dfrac{3w_{\eta,2}}{4}, \\ w_{\eta,1} = w_{\eta,1}, w_{\eta,2} = w_{\eta,2}, w_{\tau,1} = 0, w_{\tau,2} = 0 \end{matrix}\right\}. \tag{3.38}$$

Substituting (3.38) into (3.37) yields

$$f = w_{3,f}\Big(w_{1,3}\sec\big(- \frac{3}{4}\chi w_{\eta,1} + \eta w_{\eta,1}\big) + w_{2,3}\operatorname{arccot}\big(- \frac{3}{4}\chi w_{\eta,2} + \eta w_{\eta,2}\big)\Big)^2 + b_4. \tag{3.39}$$

Substituting (3.39) into (2.9), one obtains group invariant solution u_{10}:

$$\begin{aligned} u_{10} = \ & w_{3,f}\Big(w_{1,3}\sec\Big(- \frac{3}{4}(-\frac{t^2}{2} + x)w_{\eta,1} + (-t + y)w_{\eta,1}\Big) \\ & + w_{2,3}\operatorname{arccot}\big(- \frac{3}{4}(-\frac{t^2}{2} + x)w_{\eta,2} + (-t + y)w_{\eta,2}\big)\Big)^2 + t^2 - 2tz + b_4. \end{aligned} \tag{3.40}$$

Choosing appropriate parameters, the dynamic characteristics of u_{10} are intuitively illustrated in Figure 12.

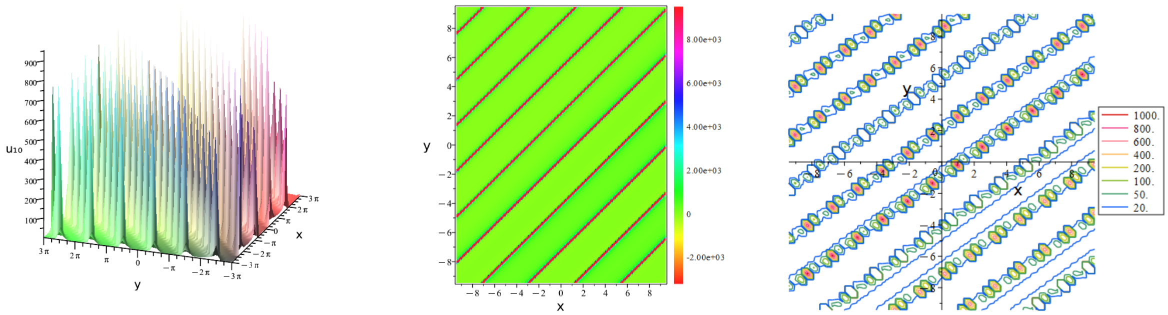

(a) 3D plot (b) density plot (c) contour plot

Figure 12. The profiles of solution u_{10}, with $z=1, t=1, b_4=2, w_{3,f}=1, w_{1,3}=1, w_{2,3}=1, w_{\eta,1}=1, w_{\eta,2}=1$.

3.2.5. Case 5

Following the formula (2.15) of **model [3,2,2,1]**, when suppose $F_1(\theta_1)=\theta_1,\ F_2(\theta_2)=(\theta_2)^2,$ $F_3(\theta_3)=\ln(\theta_3),\ F_4(\theta_4)=\mathrm{JacobiCN}(\theta_4,\frac{3}{5}),\ b_4=0$, the test function is:

$$f = w_{3,f}\ln\Big(w_{1,3}(\theta_1)+w_{2,3}(\theta_2)^2+b_3\Big)+w_{4,f}\,\mathrm{JacobiCN}\Big(w_{1,4}(\theta_1)+w_{2,4}(\theta_2)^2,\frac{2}{5}\Big)+b_5. \tag{3.41}$$

Substituting (3.41) into the Eq. (2.10) derives 36 sets of solutions, one of which is expressed as

$$\left\{\begin{aligned}&w_{1,3}=w_{1,3}, w_{1,4}=0, w_{2,3}=w_{2,3}, w_{2,4}=w_{2,4}, w_{3,f}=w_{3,f}, w_{4,f}=w_{4,f},\\ &w_{\chi,1}=-\frac{3w_{\eta,1}}{4}, w_{\chi,2}=-\frac{3w_{\eta,2}}{4}, w_{\eta,1}=w_{\eta,1}, w_{\eta,2}=w_{\eta,2}, w_{\tau,1}=0, w_{\tau,2}=0\end{aligned}\right\}. \tag{3.42}$$

Substituting (3.42) into (3.41) yields

$$\begin{aligned} f =\ & w_{3,f}\ln\Big(w_{1,3}\Big(-\frac{3}{4}\chi w_{\eta,1}+\eta w_{\eta,1}\Big)+w_{2,3}\Big(-\frac{3}{4}\chi w_{\eta,2}+\eta w_{\eta,2}\Big)^2+b_3\Big)\\ & +w_{4,f}\,\mathrm{JacobiCN}\Big(w_{2,4}\Big(-\frac{3}{4}\chi w_{\eta,2}+\eta w_{\eta,2}\Big)^2,\frac{3}{5}\Big)+b_5. \end{aligned} \tag{3.43}$$

Substituting (3.43) into (2.9), one obtains group-invariant solution u_{11}:

$$\begin{aligned} u_{11} =\ & w_{3,f}\ln\Big(w_{1,3}\Big(-\frac{3}{4}(-\frac{t^2}{2}+x)w_{\eta,1}+(-t+y)w_{\eta,1}\Big)\\ & +w_{2,3}\Big(-\frac{3}{4}(-\frac{t^2}{2}+x)w_{\eta,2}+(-t+y)w_{\eta,2}\Big)^2+b_3\Big)\\ & +w_{4,f}\,\mathrm{JacobiCN}\Big(w_{2,4}\Big(-\frac{3}{4}(-\frac{t^2}{2}+x)w_{\eta,2}+(-t+y)w_{\eta,2}\Big)^2,\frac{3}{5}\Big)+t^2-2tz+b_5. \end{aligned} \tag{3.44}$$

Choosing appropriate parameters, the characteristics of u_{11} are vividly depicted in Figure 13.

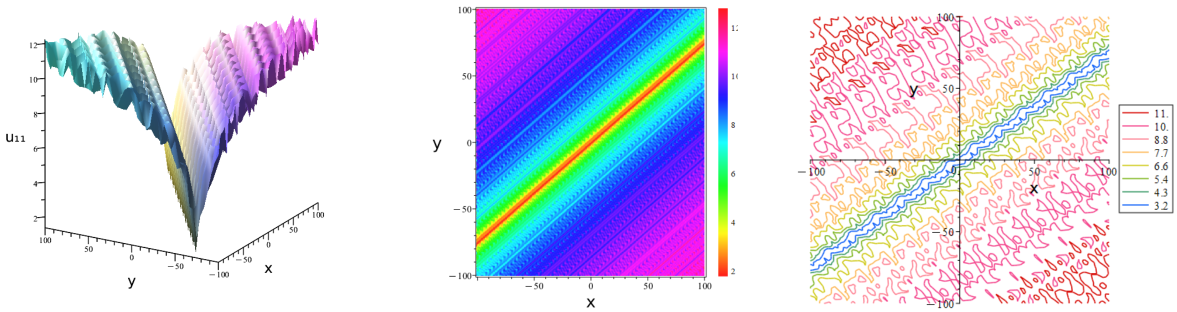

(a) 3D plot (b) density plot (c) contour plot

Figure 13. The profiles of solution u_{11}, with $z = 1, t = 1, b_3 = 2, b_5 = 2, w_{3,f} = 1, w_{4,f} = 1, w_{1,3} = 1, w_{2,3} = 1, w_{2,4} = 1, w_{\eta,1} = 1, w_{\eta,2} = 1$.

3.2.6. Case 6

Following the formula (2.16) of **model [3,3,3,1]**, we set the weight coefficients of the neural network model with appropriate values for simplicity: $w_{1,4} = 1$, $w_{2,4} = 1$, $w_{3,4} = 1$, $w_{1,5} = 1$, $w_{2,5} = 1$, $w_{3,5} = 1$, $w_{1,6} = 1$, $w_{2,6} = 1$, $w_{3,6} = 1$. When suppose activation functions $F_1(\theta_1) = \theta_1$, $F_2(\theta_2) = (\theta_2)^2$, $F_3(\theta_3) = (\theta_3)^3$, $F_4(\theta_4) = \cos(\theta_4)$, $F_5(\theta_5) = \operatorname{sech}(\theta_5)$, $F_6(\theta_6) = \tanh(\theta_6)$, the test functions can be written as

$$f = w_{4,f} \cos\left(\theta_1 + \theta_2^2 + \theta_3^3\right) + w_{5,f} \operatorname{sech}\left(\theta_1 + \theta_2^2 + \theta_3^3\right) + w_{6,f} \tanh\left(\theta_1 + \theta_2^2 + \theta_3^3\right) + b_7. \quad (3.45)$$

Substituting (3.45) into the Eq. (2.10) derives 7 sets of solutions, one of which is expressed as

$$\left\{\begin{aligned} & w_{4,f} = w_{4,f},\ w_{5,f} = w_{5,f},\ w_{6,f} = w_{6,f},\ w_{\chi,1} = -\frac{3w_{\eta,1}}{4},\ w_{\eta,1} = w_{\eta,1},\ w_{\tau,1} = 0, \\ & w_{\chi,2} = -\frac{3w_{\eta,2}}{4},\ w_{\eta,2} = w_{\eta,2},\ w_{\tau,2} = 0,\ w_{\chi,3} = -\frac{3w_{\eta,3}}{4},\ w_{\eta,3} = w_{\eta,3},\ w_{\tau,3} = 0 \end{aligned}\right\}. \quad (3.46)$$

Substituting (3.46) into (3.45) yields:

$$\begin{aligned} f = \ & w_{4,f} \cos\left(Rw_{\eta,1} + (Rw_{\eta,2})^2 + (Rw_{\eta,3})^3\right) + w_{5,f} \operatorname{sech}\left(Rw_{\eta,1} + (Rw_{\eta,2})^2 + (Rw_{\eta,3})^3\right) \\ & + w_{6,f} \tanh\left(Rw_{\eta,1} + (Rw_{\eta,2})^2 + (Rw_{\eta,3})^3\right) + b_7, \end{aligned} \quad (3.47)$$

where $R = -\frac{3\chi}{4} + \eta$. Substituting (3.47) into (2.9) and supposing parameters $w_{4,f} = 1$, $w_{5,f} = 1$, $w_{6,f} = 1$, $w_{\eta,1} = 1$, $w_{\eta,2} = 1$, $w_{\eta,3} = 1$, one obtains group-invariant solution u_{12}:

$$u_{12} = \cos(S + S^2 + S^3) + \operatorname{sech}(S + S^2 + S^3) + \tanh(S + S^2 + S^3) + t^2 - 2tz + b_7, \quad (3.48)$$

where $S = \frac{3}{8}t^2 - \frac{3}{4}x - t + y$. Choosing appropriate parameters, the properties of u_{12} are visually presented in Figure 14.

3.3. Main results

According to the above description, we obtained the following results.

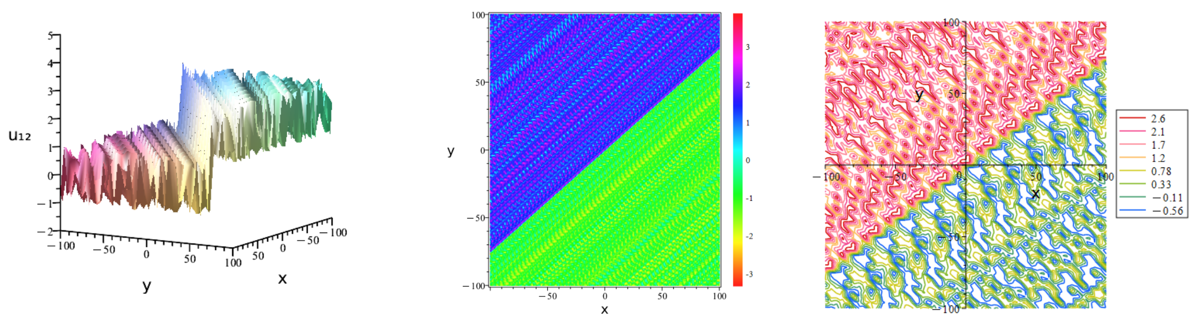

(a) 3D plot (b) density plot (c) contour plot

Figure 14. The profiles of solution u_{12}, with $z = 1, t = 1, b_7 = 2$.

Theorem 3.1. *By using the LSNNM method shown in Figure 1,* 12 *novel exact analytical solutions of the (3+1)-dimensional pYTSF equation (1.1) are achieved, noted as* u_1-u_{12} *corresponding to 12 formulas. Among them, six group-invariant solutions* u_1-u_6 *are derived from the reduction equation (2.6), and six group-invariant solutions* u_7-u_{12} *are derived from the reduction equation (2.10).*

It is easy to verify that the u_1-u_{12} corresponding to expressions (3.4), (3.8), (3.12), (3.16), (3.20), (3.24), (3.28), (3.32), (3.36), (3.40), (3.44) and (3.48) are the solutions by substituting them into Eq. (1.1), we omit this process.

Remark 3.1. It should be noted that each network model yields more than one solution. This paper only presents a new solution that is different from previous works. For each solution, the weight coefficients $w_{i,j}$ and bias b_j can be arbitrarily assigned to suitable values corresponding to specific physical problems, thereby expanding the range of possible solutions.

Remark 3.2. 12 solutions are categorized into two classes: 10 real-valued solutions (u_1, u_2, u_5-u_{12}) and 2 complex-valued solutions (u_3, u_4). By selecting appropriate parameter values, partial dynamical features of the 12 solutions are graphically demonstrated in Figures 3-18.

Remark 3.3. Some real-valued solutions which are obtained by setting activation functions as trigonometric, hyperbolic, logarithmic, exponential or Jacobi elliptic functions, exhibit certain singularity. In fact, u_1, u_2, u_8 and u_{10} are singular solutions, when using them to represent specific physical phenomena, it is necessary to consider the range of values for the variables.

Remark 3.4. It is verified that the real part of u_3 and u_4 are also solutions of Eq. (1.1). Thus, we analyze the dynamic properties of them according to the real-part plots. For solution u_3, we take the parameter n as positive integers, a negative integer, a negative irrational number, and a negative fraction to investigate its dynamic properties in Figure 5. The profiles of u_3 gradually presents a ring consisting of n lump-like wave as n increases. For example, when n takes positive values, the peak of lump-like wave is located inside the ring, while the valley of lump-like wave is outside the ring. Conversely, when n takes negative values, the peak of lump-like wave is outside the ring, and the valley of lump-like wave is inside the ring. For solution u_4 in Figure 6, the real part profiles of u_4 are a parallelogram-like shape formed by lump-like waves. We can elucidated that weight coefficients $w_{1,3}$, $w_{2,3}$ determine the number of lump-like wave in different sides of parallelogram-like shape.

4. Conclusion

Obtaining analytical solutions for high-dimensional NLPDEs has always been a challenging task. In previous work, some co-authors of this paper employed Lie symmetry analysis to study several high-dimensional, high-order NLPDEs. For most such equations, although Lie symmetry reduction can lower their dimension or order, the reduced equations often exhibit nonlinearity and non-autonomous, making them still difficult to find analytical solutions. Zhang et al., leveraging the strong expressive power of neural networks, proposed the Bilinear Neural Network method and successfully obtained analytical solutions for multiple equations [41,47–49]. Inspired by their work, we combine the Lie symmetry analysis method and neural network models, proposing the Lie-symmetry neural network method (LSNNM). We apply LSNNM to solving the (3+1)-dimensional pYTSF equation and successfully obtain a series of new analytical solutions.

As shown in Figures 3-18, all solutions exhibit distinct characteristics and possess rich dynamical features. They are helpful for accurately understanding the complex physical processes and phenomena described by Eq. (1.1) in fluid dynamics, plasma physics, optics, atmospheric oceanography, etc. Besides, complex-valued solutions play a pivotal role in describing waves, and are powerful tools for gaining a deeper understanding of complex physical phenomena in various scientific fields [20,32], especially in fluid dynamics. Moreover, these solutions verify the correctness and feasibility of the new LSNNM.

The LSNNM do not depend on the specific model and it can be used to other high-dimensional NLPDEs. The advantages of this method are threefold:

1. Equation Simplification: Before constructing solutions using neural networks, the equation is simplified to obtain some reduced equations. Since the reduced equations are derived from rigorous mathematical theory, it guarantees that any solution found based on the reduced equation is indeed a solution of the original equation.

2. Dimensionality Reduction: The reduced equation lowers the dimension of the problem (which can be further reduced by additional reductions). This significantly reduces the complexity for the subsequent neural-network-based solution construction. Within a given neural network framework, adding one input variable increases the number of corresponding weights based on the number of subsequent hidden layers. Multi-layer composition further increases computational complexity. Therefore, reducing the number of input variables plays a crucial role in the solution procedure.

3. Leveraging Neural Network Expressivity: Utilizing the strong expressive power of neural networks to construct solution forms, while delegating complex computations to mathematical software, facilitates the discovery of new analytical solutions. We can not only obtain diverse solution structures by designing different neural network architectures and selecting various activation functions, but also specifically avoid those known solutions.

In summary, this method has significant advantages in solving high-dimensional nonlinear PDEs. It has overcome many difficulties in solving high-dimensional equations even after reduction, and by reducing the dimensionality, it simplifies the complexity of network representation, thereby facilitating equation solving. More importantly, through neural networks, various types of basis functions can be freely combined or constructed based on the background of the actual problem, thus greatly expanding the scope of understanding.

However, the approach still has some potential for improvement. First, we attempt to construct neural network models with more hidden layers and general activation functions in order to obtain more extensive and informative solutions. Second, the coefficient solutions of algebraic equations often contain a large number of trivial solutions, and extracting meaningful solutions requires a significant amount of time. Designing reasonable algorithms for discrimination to filter out unimportant solutions is an important measure to improve efficiency. Additionally, by combining specific practical problems, we will focus on the selection of neuron activation functions to construct appropriate solutions, which is our subsequent key research direction.

Acknowledgments

The authors extend sincere thanks to the reviewers for their constructive suggestions. This work is supported by the National Natural Science Foundation of China (No. 11561034) and Yunnan Fundamental Research Projects (No. 202401AT070395, No. 202501AT070317).

References

[1] M. J. Ablowitz and H. Segur, *Solitons and the inverse scattering transform*, Soc. Ind. Appl. Math., 1981.

[2] O. D. Adeyemo, C. M. Khalique, Y. S. Gasimov and F. Villecco, *Variational and non-variational approaches with Lie algebra of a generalized (3+1)-dimensional nonlinear potential Yu-Toda-Sasa-Fukuyama equation in engineering and physics*, Alex. Eng. J., 2023, 63, 17–43.

[3] R. Archana and P. S. E. Jeevaraj, *Deep learning models for digital image processing: A review*, Artif. Intell. Rev., 2024, 57(1), 11.

[4] G. W. Bluman and Z. Z. Yang, *A symmetry-based method for constructing nonlocally related partial differential equation systems*, J. Math. Phys., 2013, 54(9), 806.

[5] S. J. Chen, Y. H. Yin, W. X. Ma and X. Lü, *Abundant exact solutions and interaction phenomena of the (2+1)-dimensional YTSF equation*, Anal. Math. Phys., 2019, 9, 2329–2344.

[6] S. Choubey and G. P. Karmakar, *Artificial intelligence techniques and their application in oil and gas industry*, Artif. Intell. Rev., 2021, 54(5), 3665–3683.

[7] P. A. Clarkson and M. D. Kruskal, *New similarity reductions of the Boussinesq equation*, J. Math. Phys., 1989, 30(10), 2201–2213.

[8] G. F. Deng, Y. T. Gao, J. J. Su and C. C. Ding, *Multi-breather wave solutions for a generalized (3+1)-dimensional Yu-Toda-Sasa-Fukuyama equation in a two-layer liquid*, Appl. Math. Lett., 2019, 98, 177–183.

[9] T. Fang and Y. H. Wang, *Lump-stripe interaction solutions to the potential Yu-Toda-Sasa-Fukuyama equation*, Anal. Math. Phys., 2019, 9, 1481–1495.

[10] Y. Y. Feng and S. Bilige, *Multiple rogue wave solutions of (2+1)-dimensional YTSF equation via Hirota bilinear method*, Waves Random Complex Media, 2024, 34(1), 94–110.

[11] R. T. Forestano, K. T. Matchev, K. Matcheva, A. Roman, E. B. Unlu and S. Verner, *Discovering sparse representations of Lie groups with machine learning*, Phys. Lett. B, 2023, 844, 138086.

[12] R. T. Forestano, K. T. Matchev, K. Matcheva, A. Roman, E. B. Unlu and S. Verner, *Accelerated discovery of machine-learned symmetries: Deriving the exceptional Lie groups G2, F4 and E6*, Phys. Lett. B, 2023, 847, 138266.

[13] M. Foroutan, J. Manafian and A. Ranjbaran, *Lump solution and its interaction to (3+1)-D potential-YTSF equation*, Nonlinear Dyn., 2018, 92(4), 2077–2092.

[14] H. Gao, L. N. Sun and J. X. Wang, *PhyGeoNet: Physics-informed geometry-adaptive convolutional neural networks for solving parameterized steady-state PDEs on irregular domain*, J. Comput. Phys., 2021, 428, 110079.

[15] K. Hornik, M. Stinchcombe and H. White, *Universal approximation of an unknown mapping and its derivatives using multilayer feedforward networks*, Neural Netw., 1990, 3(5), 551–560.

[16] Y. J. Hu, H. L. Chen and Z. D. Dai, *New kink multi-soliton solutions for the (3+1)-dimensional potential-Yu-Toda-Sasa-Fukuyama equation*, Appl. Math. Comput., 2014, 234, 548–556.

[17] L. Huang, J. Manafian, G. Singh, K. S. Nisar and M. K. M. Nasution, *New lump and interaction soliton, N-soliton solutions and the LSP for the (3+1)-D potential-YTSF-like equation*, Results Phys., 2021, 29, 104713.

[18] N. H. Ibragimov and R. N. Ibragimov, *Applications of Lie Group Analysis in Geophysical Fluid Dynamics*, Higher Education Press, 2011.

[19] O. A. Ilhan and J. Manafian, *A study of the wave dynamics for the reaction-diffusion Brusselator system and RKL equation*, Discrete. Dyn. Nat. Soc., 2025, 2025(1), 5188579.

[20] H. F. Ismael, İ. Okumuş, T. Aktürk, H. Bulut and M. S. Osman, *Analyzing study for the 3D potential Yu-Toda-Sasa-Fukuyama equation in the two-layer liquid medium*, J. Ocean Eng. Sci., 2024, 9(5), 454–460.

[21] D. J. Korteweg and G. de Vries, *XLI. On the change of form of long waves advancing in a rectangular canal, and on a new type of long stationary waves*, Lond. Edinb. Dubl. Phil. Mag., 1895, 39(240), 422–443.

[22] S. Kumar, K. S. Nisar and M. Niwas, *On the dynamics of exact solutions to a (3+1)-dimensional YTSF equation emerging in shallow sea waves: Lie symmetry analysis and generalized Kudryashov method*, Results Phys., 2023, 48, 106432.

[23] D. Levi and R. Benguria, *Bäcklund transformations and nonlinear differential difference equations*, Proc. Natl. Acad. Sci., 1980, 77(9), 5025–5027.

[24] W. T. Li and B. Li, *Construction of degenerate lump solutions for (2+1)-dimensional Yu-Toda-Sasa-Fukuyama equation*, Chaos, Solitons & Fractals, 2024, 180, 114572.

[25] Y. N. Li, J. Manafian, S. F. S. Takami, Z. M. Shatouri, F. A. Alenizi, A. H. Alawadi and A. Alsaalamy, *Study of the modulational instability and miscellaneous soliton for metamaterials via three powerful schemes*, J. Nonlinear Opt. Phys. & Mater., 2025, 34(3), 2350090.

[26] Z. T. Li and Z. D. Dai, *Exact periodic cross-kink wave solutions and breather type of two-solitary wave solutions for the (3+1)-dimensional potential-YTSF equation*, Comput. Math. Appl., 2011, 61(8), 1939–1945.

[27] S. K. Liu, Z. T. Fu, S. D. Liu and Q. Zhao, *Jacobi elliptic function expansion method and periodic wave solutions of nonlinear wave equations*, Phys. Lett. A, 2001, 289(1–2), 69–74.

[28] J. M. Luo, J. Manafian, A. Aghazadeh, O. A. Ilhan, B. Eslami, A. A. Fattah, K. H. Mahmoud and M. F. Aghdaei, *Study of phase separation process in multi-component mixtures using analytical methods and decomposition variational iteration method for the fourth-order Cahn–Hilliard equation*, Sci. Rep., 2025, 15(1), 38789.

[29] V. B. Matveev, *Darboux transformation and explicit solutions of the kadomtcev-petviaschvily equation, depending on functional parameters*, Lett. Math. Phys., 1979, 3(3), 213–216.

[30] E. Noether, *Invariant variation problems*, Transp. Theory Stat. Phys., 1971, 1(3), 186–207.

[31] M. Raissi, P. Perdikaris and G. E. Karniadakis, *Physics-informed neural networks: A deep learning framework for solving forward and inverse problems involving nonlinear partial differential equations*, J. Comput. Phys., 2019, 378, 686–707.

[32] A. S. Rashed, M. Inc and R. Saleh, *Extensive novel waves evolution of three-dimensional Yu-Toda-Sasa-Fukuyama equation compatible with plasma and electromagnetic applications*, Mod. Phys. Lett. B, 2023, 37(01), 2250195.

[33] D. Ray, J. Murgoitio-Esandi, A. Dasgupta and A. A. Oberai, *Solution of physics-based inverse problems using conditional generative adversarial networks with full gradient penalty*, Comput. Methods Appl. Mech. Eng., 2023, 417, 116338.

[34] S. T. R. Rizvi, K. Ali, U. Akram, S. O. Abbas, A. Bekir and A. R. Seadawy, *Stability analysis and solitary wave solutions for Yu Toda Sasa Fukuyama equation*, Nonlinear Dyn., 2025, 113(3), 2611–2623.

[35] F. Schwarz, *Symmetries of differential equations: From Sophus Lie to computer algebra*, SIAM Rev., 1988, 30(3), 450–481.

[36] R. Y. Shao, J. Manafian, O. A. İlhan, K. H. Mahmoud, B. A. Alreda and A. S. A. Alsubaie, *Computational study of thin films made from the ferroelectric materials with Paul Painlevé approach and expansion and variational methods*, Sci. Rep., 2024, 14(1), 29039.

[37] J. Sirignano and K. Spiliopoulos, *DGM: A deep learning algorithm for solving partial differential equations*, J. Comput. Phys., 2018, 375, 1339–1364.

[38] S. R. Svirshchevskii, *Lie-Bäcklund symmetries of linear ODEs and generalized separation of variables in nonlinear equations*, Phys. Lett. A, 1995, 199(5–6), 344–348.

[39] M. L. Wang and X. Z. Li, *Applications of F-expansion to periodic wave solutions for a new Hamiltonian amplitude equation*, Chaos, Solitons & Fractals, 2005, 24(5), 1257–1268.

[40] X. Y. Wu, Y. Q. Yuan and Z. Du, *Resonant interactions between lumps/rogue waves and solitons for the (3+1)-dimensional Yu-Toda-Sasa-Fukuyama equation*, Nonlinear Dyn., 2023, 111(15), 14395–14408.

[41] X. R. Xie and R. F. Zhang, *Neural network-based symbolic calculation approach for solving the Korteweg-de Vries equation*, Chaos, Solitons & Fractals, 2025, 194, 116232.

[42] Y. H. Xu, J. Manafian, O. A. Ilhan, A. Aghazadeh, A. A. Fattah, K. H. Mahmoud, R. A. Barhe and W. D. Kadhim, *Conservation law, stability analysis, degenerate lump and traveling wave solutions for (2+1)-dimensional KP-BBM equation*, Qual. Theor. Dyn. Syst., 2025, 24(6), 1–54.

[43] Z. Y. Yan, *New families of nontravelling wave solutions to a new (3+1)-dimensional potential-YTSF equation*, Phys. Lett. A, 2003, 318(1–2), 78–83.

[44] S. J. Yu, K. Toda, N. Sasa and T. Fukuyama, *N soliton solutions to the Bogoyavlenskii Schiff equation and a quest for the soliton solution in (3+1) dimensions*, J. Phys. A: Math. Gen., 1998, 31(14), 3337.

[45] X. H. Yu and D. W. Zuo, *Breather and soliton solutions of a generalized (3+1)-dimensional Yu-Toda-Sasa-Fukuyama equation*, Phys. Fluids, 2024, 36(3), 037110.

[46] X. P. Zeng, Z. D. Dai and D. L. Li, *New periodic soliton solutions for the (3+1)-dimensional potential-YTSF equation*, Chaos, Solitons & Fractals, 2009, 42(2), 657–661.

[47] R. F. Zhang and S. Bilige, *Bilinear neural network method to obtain the exact analytical solutions of nonlinear partial differential equations and its application to p-gBKP equation*, Nonlinear Dyn., 2019, 95, 3041–3048.

[48] R. F. Zhang and M. C. Li, *Bilinear residual network method for solving the exactly explicit solutions of nonlinear evolution equations*, Nonlinear Dyn., 2022, 108(1), 521–531.

[49] R. F. Zhang, M. C. Li, J. Y. Gan, Q. Li and Z. Z. Lan, *Novel trial functions and rogue waves of generalized breaking soliton equation via bilinear neural network method*, Chaos, Solitons & Fractals, 2022, 154, 111692.

[50] T. X. Zhang, H. N. Xuan, D. F. Zhang and C. J. Wang, *Non-travelling wave solutions to a (3+1)-dimensional potential-YTSF equation and a simplified model for reacting mixtures*, Chaos, Solitons & Fractals, 2007, 34(3), 1006–1013.

[51] X. Zhao, L. M. Wang, Y. F. Zhang, X. M. Han, M. Deveci and M. Parmar, *A review of convolutional neural networks in computer vision*, Artif. Intell. Rev., 2024, 57(4), 99.

[52] Y. Zhao, B. Tian, H. Y. Tian, D. Y. Yang and Y. Shen, *Gram-type, breather and hybrid solutions for the (3+1)-dimensional potential Yu-Toda-Sasa-Fukuyama equation in a two-layer liquid*, Nonlinear Dyn., 2023, 111(17), 16353–16365.

[53] Z. L. Zhao and L. C. He, *Multiple lump solutions of the (3+1)-dimensional potential Yu-Toda-Sasa-Fukuyama equation*, Appl. Math. Lett., 2019, 95, 114–121.

[54] R. Z. Zhdanov, *Conditional Lie-Backlund symmetry and reduction of evolution equations*, J. Phys. A: Math. Gen., 1995, 28(13), 3841.

Received October 2025; Accepted May 2026; Available online August 2026.